PŮVODNÍ PRÁCE/ORIGINAL PAPER

Bendadaite from Krásno near Horní Slavkov (Czech Republic), description and Raman spectroscopy

Jiří Sejkora[1)]*, Jaromír Tvrdý[2,3)], Jiří Čejka[1)], Luboš Vrtiška[1)] a Zdeněk Dolníček[1)]

[1)]*Department of Mineralogy and Petrology, National Museum, Cirkusová 1740, 193 00 Praha 9 - Horní Počernice;*
**e-mail: jiri_sejkora@nm.cz*
[2)]*Azalková 522, 460 15 Liberec*
[3)]*Department of Geology, Faculty of Science, Masaryk University, Kotlářská 267/2, 611 37 Brno*

Sejkora J, Tvrdý J, Čejka J, Vrtiška L, Dolníček Z (2019) Bendadaite from Krásno near Horní Slavkov (Czech Republic), description and Raman spectroscopy. Bull Mineral Petrolog 27(1): 63-71 ISSN 2570-7337

Abstract

A rare Fe^{2+}-Fe^{3+} dominant arsenate of the arthurite group, bendadaite, was determined at two samples from an abandoned Huber open pit in the Krásno ore district near Horní Slavkov, Slavkovský les area (Czech Republic). Bendadaite occurs there as brownish to olive green crystalline aggregates up to 2 - 6 mm in size in cavities of quartz gangue. The aggregates are composed by elongate prismatic crystals up to 100 - 200 μm in length, partly in radial arrangement. It is opaque to semi-translucent (aggregates) to translucent (thin fragments). It has vitreous to subadamantine (crystals) or greasy to dull (aggregates) lustre. Bendadaite is monoclinic, space group $P2_1/c$, with the unit-cell parameters refined from X-ray powder diffraction data: *a* 10.183(2), *b* 9.672(2), *c* 5.536(1) Å, *β* 94.15(2)°, *V* 543.8(1) Å^3 (sample NM) and *a* 10.175(2), *b* 9.682(2), *c* 5.532(1) Å, *β* 94.13(2)°, *V* 543.6(1) Å^3 (sample JT). The chemical composition of bendadaite agrees with general stoichiometry of the arthurite group minerals and corresponds to the following empirical formulae: $(Fe_{0.52}Zn_{0.25}Cu_{0.02}Mg_{0.02}\square_{0.19})_{\Sigma 1.00}(Fe^{3+}_{1.80}Al_{0.20})_{\Sigma 2.00}[(AsO_4)_{1.66}(PO_4)_{0.34}]_{\Sigma 2.00}(OH)_2 \cdot 4H_2O$ (sample NM) and $(Fe_{0.63}Zn_{0.26}\square_{0.11})_{\Sigma 1.00}(Fe^{3+}_{1.87}Al_{0.13})_{\Sigma 2.00}[(AsO_4)_{1.62}(PO_4)_{0.38}]_{\Sigma 2.00}(OH)_2 \cdot 4H_2O$ (sample JT). The Raman spectra of both studied bendadaite samples as well as tentative assignment of observed bands are given in this paper. Origin of bendadaite from Krásno is connected to *in-situ* supergene weathering of primary arsenopyrite, sphalerite and phosphates and high activity of arsenate and Fe^{2+}, Fe^{3+} ions in acidic supergene fluids.

Key words: *bendadaite, arthurite group, powder X-ray diffraction data, unit-cell parameters, chemical composition, Raman spectroscopy, Krásno near Horní Slavkov, Czech Republic*

Obdrženo 18. 3. 2019; přijato 14. 6. 2019

Introduction

Arthurite group minerals comprise monoclinic arsenates and phosphates with general formula $AB_2(TO_4)_2(OH,O)_2 \cdot 4H_2O$ (Table 1). The structural position A is occupied mainly by M^{2+} elements, such as Cu^{2+}, Fe^{2+}, Mn^{2+}, Zn^{2+}, Co^{2+}, Mg^{2+} and Ca^{2+} (Peacor et al. 1984; Jambor et al. 2002; Mills et al. 2008). According to Moore et al. (1974) and Kolitsch et al. (2010), also Fe^{3+} and vacancy may occur in this site. The results of crystal structure study (Keller, Hess 1978; Hughes et al. 1996; Kampf 2005; Kolitsch et al. 2010) indicate that Zn, Cu and Co enter exclusively the *A*-site. The *B*-site is occupied predominantly by Fe^{3+} and some Al^{3+} (Peacor et al. 1984; Staněk 1988; Kolitsch et al. 2010) and probably minor Ti^{4+} (Staněk 1988). The tetrahedral *T*-position may contain minor S and Si, in addition to dominanting As and P (Davis, Hey 1969; Jambor et al. 2002; Sejkora et al. 2006c).

In the Czech Republic, the P-dominant members of arthurite group are known from the Krásno ore district - earlshannonite, whitmoreite (Sejkora et al. 2006d), kunatite (Mills et al. 2008) and two unnamed phases UNK7 and UNK8 (Sejkora et al. 2006c). Earlshannonite and whitmoreite were also described from pegmatite near Dolní Bory, western Moravia (Staněk 1988, 1997) and whitmoreite from the Sn-Li deposit Vernéřov near Aš (Breiter et al. 2009). The occurrences of As-dominant members of arthurite group are very rare, they were found only at the Krásno ore district - arthurite (Vrtiška et al. 2018) and bendadaite, which is subject of this study.

Bendadaite, the Fe-Fe-As dominant member of arthurite group, was described by Kolitsch et al. (2010) as a

Table 1 *Ideal occupation of crystal-structure sites of arthurite group minerals*

	A	B	T
arthurite	Cu	Fe	As
bendadaite	Fe	Fe	As
cobaltarthurite	Co	Fe	As
ojuelaite	Zn	Fe	As
earlshannonite	Mn	Fe	P
kunatite	Cu	Fe	P
whitmoreite	Fe	Fe	P
UNK7	Zn	Fe	P
UNK8	Fe	Al	P

A, B and *T* - sites of general formula $AB_2(TO_4)_2(OH,O)_2 \cdot 4H_2O$; UNK7 and UNK8 - unnamed phases from Krásno (Sejkora et al. 2006c)

new mineral from the pegmatite occurrences Bendada (central Portugal) and Lavra do Almerindo (Minas Gerais, Brazil). Further localities are the Veta Negra mine (Copiapó, Chile), Oumlil-East (Bou Azzer, Morocco), and the Fenugi Sibiri mine, Gonnosfanadiga (Sardinia, Italy). Later, bendadaite was reported from the Kiura mining area, Japan (Matsubara et al. 2009), Villatte-Haute, Haute-Vienne, France (Meisser 2010), San Miguel de Tabagón, Galicia, Spain (Calvo 2015), and the Lavrion district, Greece (Rieck et al. 2018).

Occurrence

Bendadaite was found at the Huber open pit in the Krásno ore district near Horní Slavkov, Slavkovský les area, Czech Republic. It was identified at two samples of coarse-grained quartz gangue labelled *„beraunite"* from collection of the National Museum, Prague (catalogue number P1N 95.003 - sample NM) and private collection of Jaromír Tvrdý (Liberec - sample JT). The both samples come from the same find at 1986 (JT).

The Krásno ore district belongs to one of the most important areas of tin and tungsten mining in Central Europe (Beran, Sejkora 2006). The district is represented by greisen mineralization in several granite cupolas of the large Krušné hory (Erzgebirge) granite batholith, which is underlying metamorphic rock (mainly gneisses). The largest Sn-W deposit in this district is the Huber stock. In the past, it was mined via the Huber open pit and Huber (Stannum) shaft down to 200 m under the surface (5th level at 425 m a.s.l.). The stock is bell-shaped in section, similar to a blunt cone. At 100 m beneath the present surface, the stock is 200 x 100 m in cross-section, while at a depth of 150 m, the stock extends NE-SW and is about 400 x 250 m in cross section. The Huber stock consists basically of autometamorphosed Li-mica-topaz granite with a variable degree of greisenization. It is assumed that entire apical part of this cupola was formed by greisen and quartz veins with rich ore mineralization (Beran, Sejkora 2006). Detailed descriptions of the mineralogy (more than 230 mineral species) of the Krásno ore district were published by Beran, Sejkora (2006) and Sejkora et al. (2006a-d). More recently, the new minerals tvrdýite (Sejkora et al. 2016), krásnoite (Mills et al. 2012), and iangreyite (Mills et al. 2011) were described from this locality, which also hosts the second world occurrence of kunatite (Mills et al. 2008) and plimerite (Sejkora et al. 2011).

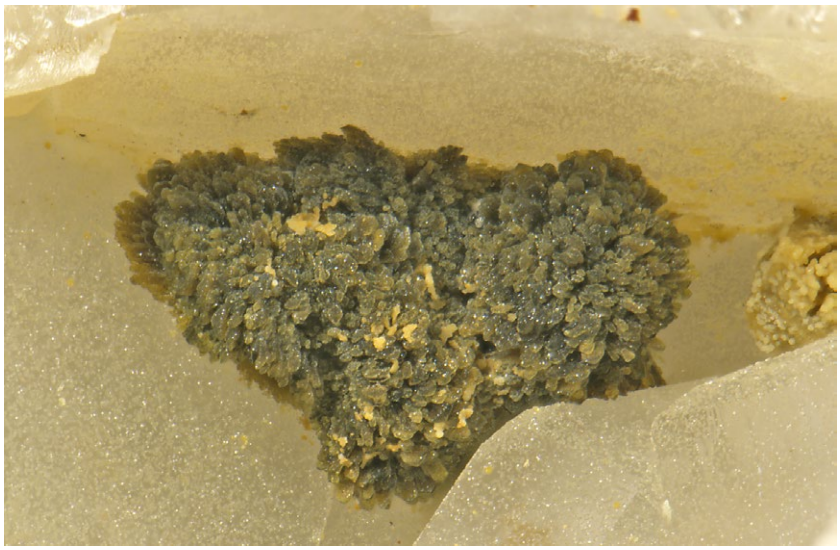

Fig. 1. *Bendadaite aggregate in cavity of quartz gangue (sample NM), Krásno near Horní Slavkov; field of view 4 mm, photo L. Vrtiška.*

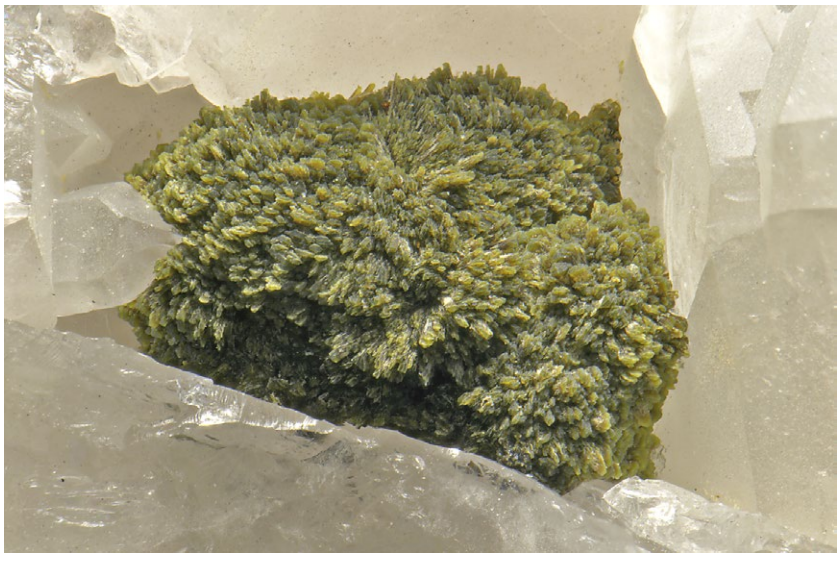

Fig. 2. *Bendadaite aggregate in cavity of quartz gangue (sample JT), Krásno near Horní Slavkov; field of view 6 mm, photo J. Sejkora.*

Morphology and physical properties

Bendadaite was identified at two samples of coarse-grained quartz gangue with abundant cavities, 8 x 8 x 7 cm (sample NM) and 8 x 6 x 2 cm (sample JT) in size. At both samples, bendadaite forms brownish to olive green crystalline aggregates up to 2 - 6 mm in size in cavities of quartz (Figs. 1 and 2). These aggregates are composed of elongated prismatic crystals up to 100 - 200 μm in length, partly in radial arrangement. Bendadaite is opaque to semi-translucent (aggregates) to translucent (thin fragments). It has vitreous to subadamantine (crystals) or greasy to dull (aggregates) lustre and greenish yellow streak. Bendadaite is brittle with irregular fracture, the good cleavage in one direction was observed. The calculated density (based on combination of empirical formula and refined unit-cell parameters) is 3.312 g/cm^3 for NM sample and 3.238 g/cm^3 for JT sample, respectively.

X-ray powder diffraction

Powder X-ray diffraction data were collected on a Bruker D8 Advance diffractometer (National Museum, Prague) with a solid-state 1D LynxEye detector using CuK_α radiation

and operating at 40 kV and 40 mA. The powder patterns were collected using Bragg–Brentano geometry in the range 3 - 60° 2θ, in 0.01° steps with a counting time of 30 s per step. Positions and intensities of reflections were found and refined using the PearsonVII profile-shape function with the ZDS program package (Ondruš 1993) and the unit-cell parameters were refined by the least-squares algorithm implemented by Burnham (1962). The experimental powder pattern was indexed in line with the calculated values of intensities obtained from the crystal structure of bendadaite (Kolitsch et al. 2010), based on Lazy Pulverix program (Yvon et al. 1977). The experimental powder data sets given in Table 2 agree well with the pattern calculated from the single-crystal data for bendadaite; experimental intensities are partly affected by preferred orientation as well as by the small amount material available for the study. The refined unit-cell parameters of bendadaite are compared in Table 3 with published data for As-dominant members of arthurite group.

Chemical composition

Samples of bendadaite were analysed with a Cameca SX-100 electron microprobe (National Museum, Prague) operating in the wavelength-dispersive mode with an accelerating voltage of 15 kV, a specimen current of 10 nA, and a beam diameter of 10 μm. The following lines and standards were used: *K*α: hematite (Fe), ZnO (Zn), diopside (Mg), rhodonite (Mn), chalcopyrite (Cu), sanidine (Al), fluorapatite (P); *L*α: clinoclase (As). Peak counting times (CT) were 20 s for main elements and 60 s for minor elements; CT for each background was one-half of the peak time. The raw intensities were converted to the concentrations automatically using *PAP* (Pouchou, Pichoir 1985) matrix-correction software. The elements Ba, Bi, Cl, Co, Cr, F, In, K, N, Na, Ni, Pb, S, Si, Sr, Th, U, V and Y were sought, but found to be below the detection limit (about 0.05-0.20 wt. %). Water content could not be analysed directly because of the minute amount of material available. The H_2O content was confirmed by Raman spectroscopy and calculated by stoichiometry of ideal formula.

Chemical composition of both studied bendadaite samples (Table 4 and 5) is very similar and agree well with the general formula of the arthurite group minerals $AB_2(TO_4)_2(OH,O)_2 \cdot 4H_2O$. The *A*-site is in both samples dominated by Fe (Fig. 3) accompanied by Zn (NM sample: 0.21 - 0.31 *apfu*; JT sample 0.20 - 0.33 *apfu*) and at NM sample also by minor contents of Cu (mean 0.02, locally up to 0.22 *apfu*) and Mg (up to 0.08 *apfu*). The results suggest that *A*-site is not fully occupied and vacancies are present on this site (up to 0.33 *pfu* in both samples). Similar situation was described for whitmoreite (More et al. 1974), cobaltarthurite (Kampf 2005) and bendadaite (Kolitsch et al. 2010). The presence of vacancy indicates a possibility that part of Fe at *A*-site is Fe^{3+} (Kolitsch et al. 2010). In addition to prevailing Fe in the *B*-site (Fig. 4), there are variable contents of Al (NM 0.07 - 0.30; JT 0.03 - 0.32 *apfu*). The tetrahedral *T*-site is dominated by As (Fig. 5) and is partly substituted by P (NM 0.16 - 0.61; JT 0.13 - 0.89

Table 2 *X-ray powder diffraction data of bendadaite from Krásno*

			sample JT			sample NM		
h	*k*	*l*	$d_{obs.}$	$I_{obs.}$	$d_{calc.}$	$d_{obs.}$	$I_{obs.}$	$d_{calc.}$
1	0	0	10.147	77.8	10.148	10.170	100.0	10.156
1	1	0	7.004	100.0	7.005	7.011	95.4	7.004
2	0	0	5.067	8.1	5.074	5.080	13.7	5.078
0	2	0	4.841	39.9	4.841	4.838	35.9	4.836
0	1	1	4.803	4.0	4.794	4.797	7.2	4.795
2	1	0	4.495	13.6	4.494	4.499	23.5	4.496
1	2	0	4.368	9.1	4.369	4.368	7.2	4.366
1	1	1	4.235	8.6	4.234	4.237	15.7	4.235
2	2	0	3.502	5.1	3.503	3.504	5.2	3.502
1	2	-1	3.481	3.0	3.478	3.477	3.3	3.478
3	0	0	3.384	4.0	3.383	3.387	6.5	3.385
2	1	1	3.384	4.0	3.381	3.387	6.5	3.382
1	3	0	3.076	9.1	3.076	3.074	8.5	3.073
2	2	-1	3.026	3.0	3.026	3.026	5.9	3.026
2	2	1	2.892	7.6	2.893	2.894	12.4	2.893
3	1	-1	2.851	6.1	2.849	2.851	13.7	2.851
3	2	0	2.773	2.0	2.773	2.775	7.8	2.773
2	3	0	2.722	13.6	2.723	2.722	15.0	2.722
1	3	1	2.661	1.5	2.662	2.660	2.0	2.660
1	1	-2	2.614	2.5	2.612	2.616	3.3	2.613
4	0	0	2.540	0.5	2.537	2.539	1.3	2.539
2	0	-2	2.4961	0.5	2.5006	2.5051	1.2	2.5026
4	1	0	2.4557	1.0	2.4542	2.4539	6.1	2.4559
3	2	1	2.4214	3.0	2.4210	2.4219	4.9	2.4214
2	3	1	2.4041	1.0	2.4054			
1	4	0	2.3548	3.0	2.3545	2.3529	2.7	2.3522
2	1	2	2.2822	0.5	2.2872	2.2894	0.8	2.2881
0	4	1	2.2168	3.0	2.2166	2.2149	4.6	2.2149
4	1	1	2.1868	1.5	2.1866	2.1885	3.6	2.1878
1	4	1	2.1523	0.5	2.1526	2.1509	1.2	2.1511
2	2	2	2.1154	1.5	2.1168	2.1136	2.0	2.1173
3	3	1	2.1154	1.5	2.1131	2.1136	2.0	2.1129
0	3	2	2.0977	1.0	2.0971	2.0962	1.4	2.0969
1	3	-2	2.0767	0.5	2.0764			
2	4	-1	2.0525	0.5	2.0532			
4	2	1	2.0352	2.0	2.0364	2.0364	3.5	2.0370
3	2	-2	2.0170	0.5	2.0162	2.0163	1.1	2.0173
5	1	0	1.9859	1.0	1.9865	1.9887	1.2	1.9879
3	4	0	1.9672	3.0	1.9685	1.9668	1.2	1.9677
4	3	-1	1.9107	1.0	1.9107	1.9112	1.2	1.9111
1	5	0	1.9025	1.0	1.9021	1.9009	2.6	1.9002
5	2	-1	1.8087	0.5	1.8095	1.8096	1.0	1.8107
2	5	1	1.7062	0.5	1.7062	1.7049	1.0	1.7050
2	4	2	1.6885	1.5	1.6875	1.6871	0.5	1.6870
3	5	0	1.6803	0.5	1.6805	1.6790	1.4	1.6796
2	1	3	1.6666	0.5	1.6655	1.6659	1.0	1.6662

apfu). The empirical formulae calculated on the basis of As+P = 2 *apfu* are following: NM sample (mean of 23 analyses): $(Fe_{0.52}Zn_{0.25}\ Cu_{0.02}Mg_{0.02}\square_{0.19})_{\Sigma 1.00}(Fe^{3+}_{1.80}Al_{0.20})_{\Sigma 2.00}[(AsO_4)_{1.66}(PO_4)_{0.34}]_{\Sigma 2.00}(OH)_2\cdot 4H_2O$, and for JT sample (mean of 29 analyses): $(Fe_{0.63}Zn_{0.26}\square_{0.11})_{\Sigma 1.00}(Fe^{3+}_{1.87}Al_{0.13})_{\Sigma 2.00}[(AsO_4)_{1.62}(PO_4)_{0.38}]_{\Sigma 2.00}(OH)_2\cdot 4H_2O$, respectively.

Raman spectroscopy

The Raman spectra (Fig. 6, Table 6) were collected in the range 4000–45 cm^{-1} using a DXR dispersive Raman Spectrometer (Thermo Scientific) mounted on a confocal Olympus microscope. The Raman signal was excited by an unpolarised red 633 nm He-Ne gas laser and detected by a CCD detector. The experimental parameters were: 100x objective, 60 s exposure time, 100 exposu-

Table 3 *Unit-cell parameters for As-dominant members of arthurite group (for monoclinic space group $P2_1/c$)*

		a [Å]	*b* [Å]	*c* [Å]	*β* [°]	*V* [Å^3]
bendadaite NM	this paper	10.183(2)	9.672(2)	5.536(1)	94.15(2)	543.8(1)
bendadaite JT	this paper	10.175(2)	9.682(2)	5.532(1)	94.13(2)	543.6(1)
bendadaite *1	Kolitsch et al. (2010)	10.239(3)	9.713(2)	5.552(2)	94.11(2)	550.7(2)
bendadaite *2	Kolitsch et al. (2010)	10.200(1)	9.718(1)	5.5432(5)	94.05(1)	548.1(1)
arthurite	Keller, Hess (1978)	10.189(2)	9.649(2)	5.598(1)	92.16(2)	549.9(2)
arthurite	Vrtiška et al. (2018)	10.102(8)	9.625(4)	5.548(4)	92.2(1)	539.1(6)
ojuelaite	Cesbron et al. (1981)	10.247(6)	9.665(5)	5.569(4)	94.36	549.37
ojuelaite	Hughes et al. (1996)	10.237(1)	9.662(3)	5.562(1)	94.36(1)	548.5
cobaltarthurite	Kampf (2005)	10.2635(9)	9.7028(8)	5.5711(5)	94.207(1)	553.30(8)
cobaltarthurite	Raudsepp, Pani (2002)	10.2694(4)	9.6790(3)	5.5723(2)	94.277(2)	552.33(3)

*1 - type locality, PXRD; *2 - cotype locality SXRD

Table 4 *Chemical composition of bendadaite (sample NM) from Krásno (wt. %)*

	mean	1	2	3	4	5	6	7	8	9	10	11	12	13
FeO	7.17	8.93	9.11	5.28	6.66	8.85	7.50	8.67	5.57	6.76	6.62	5.58	5.95	6.15
MgO	0.12	0.00	0.00	0.43	0.59	0.00	0.31	0.42	0.10	0.00	0.25	0.23	0.45	0.00
CuO	0.28	1.44	0.19	3.21	0.00	0.22	0.16	0.00	0.15	0.23	0.09	0.00	0.00	0.00
MnO	0.03	0.09	0.07	0.00	0.05	0.00	0.00	0.00	0.00	0.06	0.12	0.00	0.00	0.05
ZnO	3.88	3.58	3.55	3.15	3.69	3.58	3.66	4.32	4.00	4.27	4.36	4.77	4.22	4.69
Al_2O_3	1.97	2.52	2.61	1.55	1.73	2.86	2.48	2.21	1.39	2.09	1.80	0.71	0.99	1.76
Fe_2O_3	27.58	26.10	26.01	26.88	27.25	25.58	27.86	25.87	28.92	28.72	28.53	29.33	29.76	28.95
As_2O_5	36.66	39.84	38.96	37.21	37.32	37.12	39.39	34.24	36.25	36.09	34.93	32.81	33.19	31.64
P_2O_5	4.62	2.10	2.69	3.07	3.58	3.79	3.89	4.93	5.25	6.15	6.29	6.80	7.33	8.64
H_2O	17.30	16.95	16.98	16.53	16.90	16.95	17.91	16.55	17.54	18.05	17.68	17.17	17.66	17.88
total	99.61	101.54	100.17	97.31	97.77	98.94	103.16	97.21	99.17	102.42	100.67	97.41	99.54	99.76
Fe^{2+}	0.519	0.661	0.673	0.401	0.494	0.654	0.525	0.657	0.398	0.469	0.470	0.408	0.422	0.431
Mg	0.016	0.000	0.000	0.058	0.078	0.000	0.039	0.057	0.013	0.000	0.032	0.030	0.057	0.000
Cu	0.018	0.096	0.013	0.220	0.000	0.015	0.010	0.000	0.010	0.014	0.006	0.000	0.000	0.000
Mn	0.002	0.007	0.005	0.000	0.004	0.000	0.000	0.000	0.000	0.004	0.009	0.000	0.000	0.004
Zn	0.248	0.234	0.231	0.211	0.242	0.234	0.226	0.289	0.252	0.262	0.273	0.307	0.265	0.290
Σ *A*-site	0.804	0.997	0.922	0.890	0.818	0.903	0.800	1.002	0.673	0.750	0.788	0.745	0.744	0.725
Al	0.201	0.263	0.272	0.166	0.181	0.298	0.245	0.236	0.140	0.205	0.180	0.073	0.099	0.174
Fe^{3+}	1.799	1.737	1.728	1.834	1.819	1.702	1.755	1.764	1.860	1.795	1.820	1.927	1.901	1.826
Σ *B*-site	2.000	2.000	2.000	2.000	2.000	2.000	2.000	2.000	2.000	2.000	2.000	2.000	2.000	2.000
As	1.661	1.843	1.799	1.764	1.731	1.716	1.724	1.622	1.620	1.567	1.548	1.497	1.473	1.387
P	0.339	0.157	0.201	0.236	0.269	0.284	0.276	0.378	0.380	0.433	0.452	0.503	0.527	0.613
Σ *T*-site	2.000	2.000	2.000	2.000	2.000	2.000	2.000	2.000	2.000	2.000	2.000	2.000	2.000	2.000
OH	2.00	2.00	2.00	2.00	2.00	2.00	2.00	2.00	2.00	2.00	2.00	2.00	2.00	2.00
H_2O	4.00	4.00	4.00	4.00	4.00	4.00	4.00	4.00	4.00	4.00	4.00	4.00	4.00	4.00

Mean of 23 point analyses; 1-13 selected representative analyses; *apfu* on the base As+P = 2; H_2O and FeO/Fe_2O_3 contents were calculated on the basis of ideal formula.

res, 50 μm pinhole spectrograph aperture and 8 mW laser power level. The spectra were repeatedly acquired from different grains in order to obtain a representative spectrum with the best signal-to-noise ratio. The eventual thermal damage of the measured point was excluded by visual inspection of excited surface after measurement, by observation of possible decay of spectral features in the start of excitation and checking for thermal downshift of Raman lines. The instrument was set up by a software-controlled calibration procedure using multiple neon emission lines (wavelength calibration), multiple polystyrene Raman bands (laser frequency calibration) and standardized white-light sources (intensity calibration). Spectral manipulations were performed using the Omnic 9 software (Thermo Scientific).

In the asymmetric part of the monoclinic (space group $P2_1/c$, Z=2) bendadaite unit-cell (Kolitsch et al. 2010), there are two symmetrically distinct Fe, one $(AsO_4)^{3-}$ (partly with P substitution), two H_2O molecules and one $(OH)^-$ unit. The crystal structure of arthurite group minerals (Kampf 2005) is based upon a unique corrugated sheet of Fe^{3+}-O octahedra.

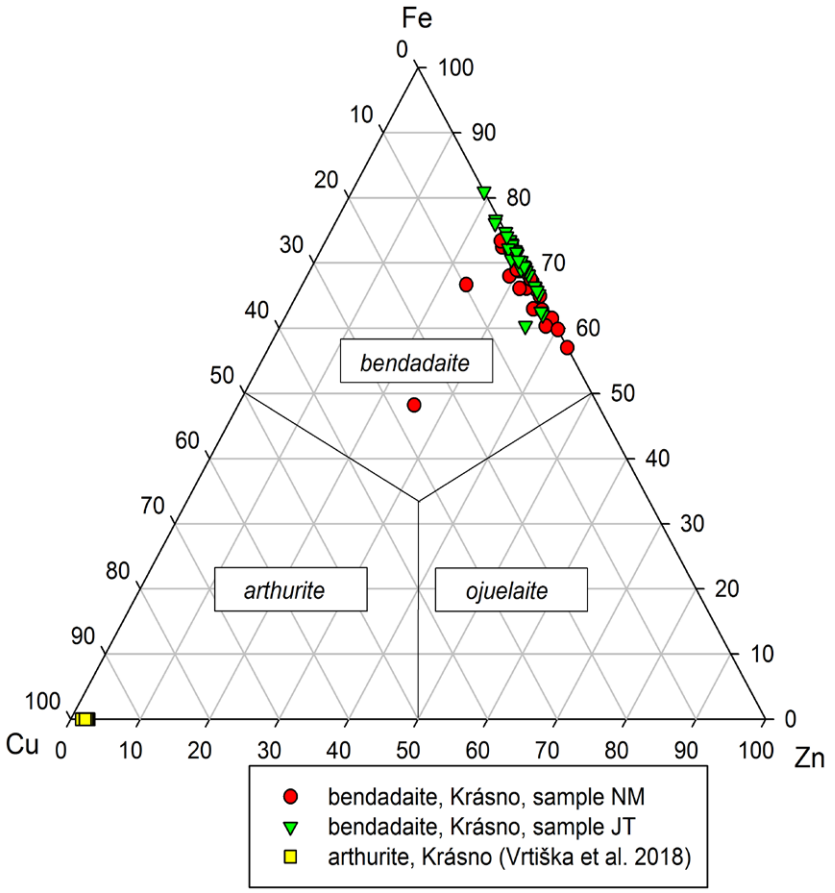

Fig. 3. *Ternary graph Zn - Fe - Cu in the A-site for As-dominant members of arthurite group from Krásno.*

Table 5 *Chemical composition of bendadaite (sample JT) from Krásno (wt. %)*

	mean	1	2	3	4	5	6	7	8	9	10	11	12	13
FeO	8.20	11.38	8.51	8.41	6.53	6.64	7.83	7.66	7.05	6.13	8.95	9.79	9.46	8.11
CuO	0.04	0.00	0.00	0.06	0.00	0.00	0.00	0.15	0.00	0.49	0.00	0.00	0.00	0.00
ZnO	3.86	3.03	3.86	2.84	3.76	3.92	4.49	3.46	3.70	4.06	4.01	4.39	4.76	4.90
Al_2O_3	1.22	2.82	1.43	0.54	0.47	1.26	1.39	0.88	0.35	1.12	1.35	2.04	2.13	1.17
Fe_2O_3	26.88	22.97	26.18	27.45	28.25	27.68	27.77	27.99	28.63	28.34	26.32	25.73	25.24	26.81
As_2O_5	33.56	36.93	37.55	37.03	36.99	36.14	34.96	33.83	33.36	34.16	31.69	30.14	26.83	22.86
P_2O_5	4.87	1.54	2.07	2.28	2.92	4.04	5.03	5.21	5.33	5.65	5.70	7.10	8.83	11.34
H_2O	16.24	15.45	16.03	15.96	16.35	16.73	16.89	16.57	16.46	16.97	16.04	16.32	16.12	16.16
total	94.88	94.12	95.63	94.57	95.27	96.41	98.36	95.74	94.88	96.92	94.06	95.52	93.37	91.35
Fe^{2+}	0.633	0.923	0.666	0.661	0.501	0.498	0.581	0.579	0.537	0.453	0.700	0.753	0.736	0.629
Cu	0.003	0.000	0.000	0.004	0.000	0.000	0.000	0.010	0.000	0.033	0.000	0.000	0.000	0.000
Zn	0.263	0.217	0.267	0.197	0.255	0.259	0.294	0.231	0.249	0.265	0.277	0.298	0.327	0.336
Σ *A*-site	0.900	1.140	0.932	0.862	0.755	0.757	0.875	0.821	0.786	0.750	0.977	1.050	1.063	0.965
Al	0.132	0.322	0.158	0.060	0.051	0.133	0.145	0.094	0.038	0.117	0.149	0.221	0.233	0.128
Fe^{3+}	1.868	1.678	1.842	1.940	1.949	1.867	1.855	1.906	1.962	1.883	1.851	1.779	1.767	1.872
Σ *B*-site	2.000	2.000	2.000	2.000	2.000	2.000	2.000	2.000	2.000	2.000	2.000	2.000	2.000	2.000
As	1.620	1.873	1.836	1.819	1.773	1.693	1.622	1.601	1.589	1.578	1.549	1.448	1.305	1.109
P	0.380	0.127	0.164	0.181	0.227	0.307	0.378	0.399	0.411	0.422	0.451	0.552	0.695	0.891
Σ *T*-site	2.000	2.000	2.000	2.000	2.000	2.000	2.000	2.000	2.000	2.000	2.000	2.000	2.000	2.000
OH	2.00	2.00	2.00	2.00	2.00	2.00	2.00	2.00	2.00	2.00	2.00	2.00	2.00	2.00
H_2O	4.00	4.00	4.00	4.00	4.00	4.00	4.00	4.00	4.00	4.00	4.00	4.00	4.00	4.00

Mean of 29 point analyses; 1-13 selected representative analyses; *apfu* on the base As+P = 2; H_2O and FeO/Fe_2O_3 contents were calculated on the basis of ideal formula.

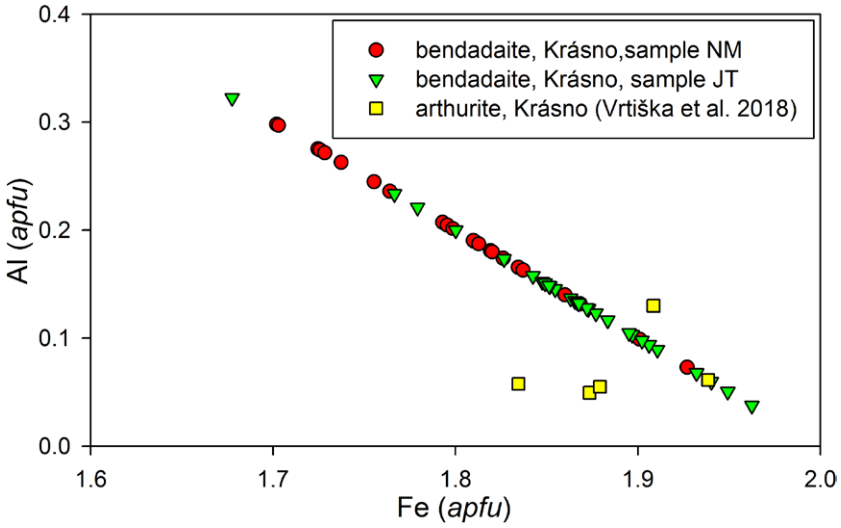

Fig. 4. *Graph Fe - Al in the B-site for As-dominant members of arthurite group from Krásno.*

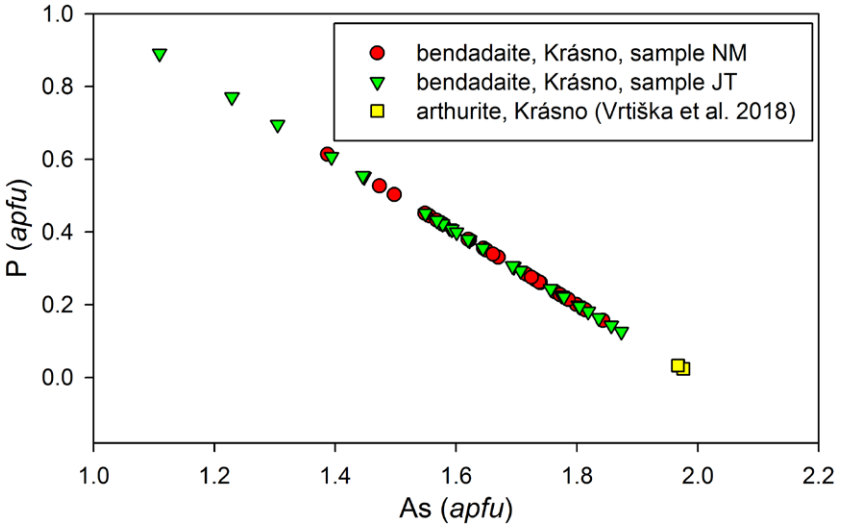

Fig. 5. *Graph As - P contents in the tetrahederal site for As-dominant members of arthurite group from Krásno.*

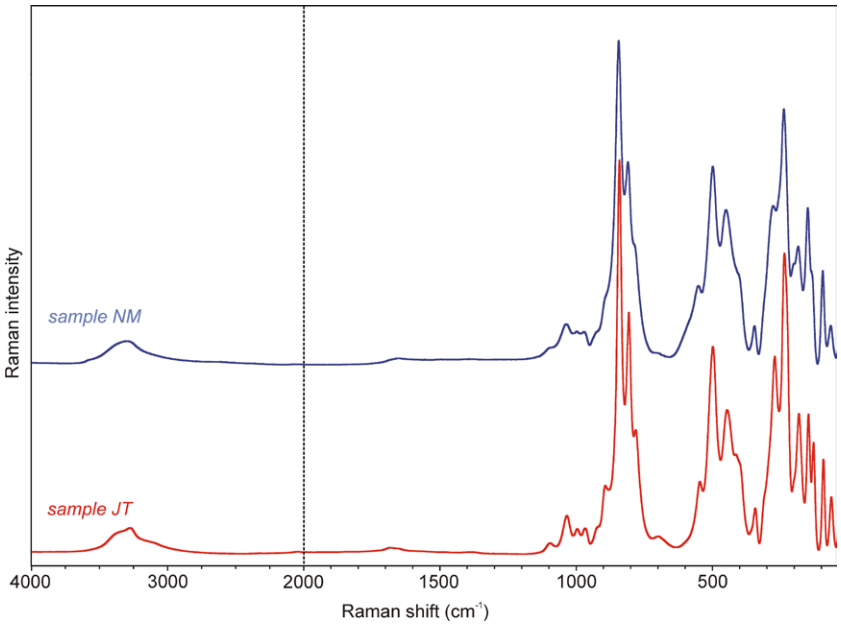

Fig. 6 *Raman spectra for bendadaite from Krásno (split at 2000 cm^{-1}).*

Each octahedron shares an edge (O1-O1) and two vertices (OH) with equivalent octahedra; two remaining vertices (O2 and O4) are shared with AsO_4 tetrahedras. Three of the four tetrahedron vertices link to octahedron vertices in the same sheet of Fe^{3+}-O octahedra, the remaining corner links to a Fe^{2+}-O octahedron. Two trans vertices of the Fe^{2+}–O octahedra link to AsO_4 tetrahedra attached to different sheets, thereby forming bridges between the sheets.

In the case of free tetrahedra $(AsO_4)^{3-}$ and $(PO_4)^{3-}$ (*T*d symmetry), there are nine normal vibrations, characterized by four fundamental modes of vibrations - ν_1 (A_1) symmetric stretching vibration, Raman active, ν_2 (δ) (E) doubly degenerate bending vibration, Raman active, ν_3 (Z_2) triply degenerate antisymmetric stretching vibration, Raman and infrared active, and ν_4 (δ) (Z_2) triply degenerate bending vibration, Raman and infrared active (Nakamoto 2009). Symmetry lowering *T*d → C_{3v}, C_{2v}, C_1 may be connected with infrared activation of infrared inactive vibrations and splitting of degenerate vibrations. For the classification of molecular vibrations, the total reducible representations decompose into $\Gamma = A_1 + E + 2F_2$ (Mielke, Ratajczak 1972; Vansant et al. 1973) vibrations. The FeO_6 octahedra XY_6 are characterized by six normal modes of vibration. The ν_1 (ν XY, A_{1g}), ν_2 (ν XY, E_g), and ν_5 (δ YXY, F_{2g}) are Raman active, whereas only ν_3 (ν XY, F_{1u}) and ν_4 (δ YXY, F_{1u}) are infrared active. The ν_6 (δ YXY, F_{2u}) is inactive in infrared and Raman spectrum (Nakamoto 2009).

Weak bands or shoulders at 3564 cm^{-1} (NM) and 3533 cm^{-1} (JT) are assigned to the ν OH stretching vibrations of weakly hydrogen-bonded hydroxyls, OH^-, while bands at 3349, 3252 and 3051 cm^{-1} (NM), and 3366, 3269 and 3136 cm^{-1} (JT) are connected with ν OH stretching vibrations of hydrogen-bonded water molecules. According to Libowitzky (1999), aproximate O-H×××O hydrogen bond lengths vary in the range from 3.06 to 2.69 Å. Bands at 1654 cm^{-1} (NM) and 1676 cm^{-1} (JT) are attributed to the ν_2 (δ) hydrogen-bonded water molecules. Bands at 1097, 1038 and 995 cm^{-1} (NM) and 1096, 1035 and 995 cm^{-1} (JT) are related to the split triply degenerate ν_3 $(PO_4)^{3-}$ antisymmetric stretching vibrations and bands at 970 cm^{-1} (NM) and 967 cm^{-1} (JT) to the ν_1 $(PO_4)^{3-}$ symmetric stretching vibrations. Any tentative assignment

of bands to the triply degenerate ν_3 $(AsO_4)^{3-}$ antisymmetric stretching vibrations makes problems. Because of the *T*d symmetry lowering, these degenerate ν_3 $(AsO_4)^{3-}$ vibrations split, the number of the observed bands may depend on the number of molecules in the unit cell (Z = 2), and the ν_3 and ν_1 $(AsO_4)^{3-}$ may coincide (Nakamoto 2009). Bands at 929, 892, 869, 810 and 782 cm^{-1} (NM) and 924, 893, 870, 807, 779 and 696 cm^{-1} (JT) may be attributed to the split ν_3 $(AsO_4)^{3-}$, however, some coincidence with libration modes of water molecules is possible. The very strong bands at 844 cm^{-1} (NM) and 841 cm^{-1} (JT) are assigned to the ν_1 $(AsO_4)^{3-}$ symmetric stretching vibrations. Bands at 552 and 499 cm^{-1} (NM) and 547 and 499 cm^{-1} (JT) are assigned to the split triply degenerate ν_4 (δ) $(PO_4)^{3-}$ out-of-plane bend. A coincidence with the δ Fe-(O,OH) bend is supposed. Bands at 447 and 402 cm^{-1} (NM) and 445, 413 and 396 cm^{-1} (JT) relates to the split triply degenerate ν_4 (δ) $(AsO_4)^{3-}$ out-of-plane bend. A probable coincidence of the bands at 447 and 445 cm^{-1}, respectively, with one of the bands assigned to the doubly degenerate ν_2 (δ) $(PO_4)^{3-}$ out-of-plane bend and δ Fe-(O,OH) bend may be also possible. Bands at 340 and 310 cm^{-1} (NM) and 344 and 311 cm^{-1} (JT) are attributed to the split doubly degenerate ν_2 (δ) $(AsO_4)^{3-}$ in-plane bend. Bands at 258, 235 and 204 cm^{-1} (NM) and 296, 279, 233 and 202 cm^{-1} (JT) are connected with ν Fe-(O,OH) stretch in Fe-$(O,OH)_6$ octahedra. Bands at 184, 149, 131, 95 and 63 cm^{-1} (NM) and 182, 147, 128, 92 and 62 cm^{-1} (JT) are attributed to lattice modes. Infrared spectrum of bendadaite was published by Kolitsch et al. (2010), infrared and Raman spectra of arthurite and cobaltarthurite by Jambor et al. (2002). All these spectra are comparable with

Table 6 *Tentative assignment of Raman spectra for bendadaite*

sample NM			sample JT			
position [cm^{-1}]	FWHM [cm^{-1}]	$I_{rel.}$	position [cm^{-1}]	FWHM [cm^{-1}]	$I_{rel.}$	tentative assignment
3564	48	1	3533	173	2	ν OH stretch of weakly hydrogen-bonded hydroxyls OH^-
3349	223	27	3366	164	23	ν OH stretch of hydrogen-bonded water molecules
3252	308	55	3269	103	22	ν OH stretch of hydrogen-bonded water molecules
3051	206	6	3136	308	41	ν OH stretch of hydrogen-bonded water molecules
1654	56	4	1676	10	1	ν_2 (δ) H_2O bend of hydrogen-bonded water molecules
1097	33	3	1096	24	2	ν_3 $(PO_4)^{3-}$ antisymmetric stretch
1038	49	18	1035	32	13	ν_3 $(PO_4)^{3-}$ antisymmetric stretch
995	30	6	995	23	4	ν_3 $(PO_4)^{3-}$ antisymmetric stretch
970	24	5	967	18	4	ν_1 $(PO_4)^{3-}$ symmetric stretch
929	24	3	924	17	2	ν_3 $(AsO_4)^{3-}$ antisymmetric stretch, H_2O libration
892	35	20	893	25	16	ν_3 $(AsO_4)^{3-}$ antisymmetric stretch
869	23	7	870	25	6	ν_3 $(AsO_4)^{3-}$ antisymmetric stretch, H_2O libration
844	27	100	841	21	100	ν_1 $(AsO_4)^{3-}$ symmetric stretch
810	25	42	807	21	47	ν_3 $(AsO_4)^{3-}$ antisymmetric stretch
782	37	36	779	30	33	ν_3 $(AsO_4)^{3-}$ antisymmetric stretch
			696	24	2	ν_3 $(AsO_4)^{3-}$ antisymmetric stretch (?), H_2O libration
552	76	54	547	34	22	δ Fe-(O,OH) bend, ν_4 (δ) $(PO_4)^{3-}$ out-of-plane bend
499	35	70	499	36	80	δ Fe-(O,OH) bend, ν_4 (δ) $(PO_4)^{3-}$ out-of-plane bend
447	51	83	445	41	59	ν_2 (δ) $(PO_4)^{3-}$ out-of-plane bend, ν_4 (δ) $(AsO_4)^{3-}$ out-of-plane bend, δ Fe-(O,OH) bend
			413	32	15	ν_4 (δ) $(AsO_4)^{3-}$ out-of-plane-bend
402	38	30	396	31	21	ν_4 (δ) $(AsO_4)^{3-}$ out-of-plane bend
346	17	7	344	18	8	ν_2 (δ) $(AsO_4)^{3-}$ in-plane bend
310	15	2	311	13	4	ν_2 (δ) $(AsO_4)^{3-}$ in-plane bend
			296	23	13	ν Fe-(O,OH) stretch
278	52	84	270	30	64	ν Fe-(O,OH) stretch
235	31	89	233	27	74	ν Fe-(O,OH) stretch
204	14	5	202	12	4	ν Fe-(O,OH) stretch
184	34	47	182	26	43	lattice modes
149	20	37	147	16	25	lattice modes
131	15	13	128	12	15	lattice modes
95	15	19	92	12	13	lattice modes
63	35	26	62	18	14	lattice modes

$I_{rel.}$ calculated from the band area.

Raman spectrum of bendadaite, presented in this paper. Kolitsch et al. (2010) observed bands and shoulders in the infrared spectrum of bendadaite: 3220, 3250, 3085 and 1643 cm^{-1} (ν OH stretch), 1092, 1045, 1033, 995 and 969 cm^{-1} (PO_4^{3-} stretch), 925, 881, 854, 811 and 768 cm^{-1} (AsO_4^{3-} stretch), 650 and 620 cm^{-1} (PO_4^{3-} bend), and 490, 467 and 431 cm^{-1} (mixed modes involving O-As-O angles and Fe-O bands. Frost et al. (2003), on the contrary, incorrectly assigned in the Raman spectra of unsatisfactory determined arthurite and whitmoreite a band at 1044 cm^{-1} to $(CO_3)^{2-}$ stretch. Palmer, Frost (2011) described infrared and Raman spectra of arthurite containing SO_4^{2-} ions (?) with proposed chemical formula $CuFe^{3+}(AsO_4,PO_4,SO_4)_2(OH)_2 \cdot 4H_2O$.

Condition of formation

The conditions of formation of bendadaite and its thermodynamic stability field appear to be restricted, with an equilibrium between Fe^{2+} and Fe^{3+} oxidation states being necessary (Kolitsch et al. 2010). At Krásno, bendadaite is formed under conditions of *in-situ* supergene zone from acidic fluids with high activity of arsenate and Fe^{2+}, Fe^{3+} ions, derived from weathering of primary arsenopyrite. The determined Zn and phosphate contents in studied bendadaite are connected with weathering of primary sphalerite and phosphates (mainly fluorapatite and triplite).

Acknowledgements

The authors wish to express their thanks to Jana Ulmanová (National Museum, Prague) for her kind support in this study. This work was financially supported by Czech Science Foundation (project GACR 17-09161S).

References

Beran P, Sejkora J (2006) The Krásno Sn-W ore district near Horní Slavkov: Mining history, geological and mineralogical characteristics. J Czech Geol Soc 51: 3 – 42

Breiter K, Škoda R, Veselovský F (2009) Unusual P-, Li- and Sn-rich pegmatite from Vernéřov near Aš, Czech Republic. Bull mineral-petrolog Odd Nár Muz (Praha) 17(1): 41-59 (in Czech)

Burnham Ch W (1962) Lattice constant refinement. Carnegie Inst Washington Year Book 61: 132-135

Calvo M (2015): Minerales y Minas de España. Vol. VII, Fosfatos, arseniatos y vanadatos. Escuela Técnica Superior de Ingenieros de Minas de Madrid - Fundación Gómez Pardo. 1-479

Cesbron F, Romero SM, Williams SA (1981) La mapimite et l`ojuélaïte, deux nouveaux arséniates hydratés de zinc et de fer de la mine Ojuela, Mapimi, Mexique. Bull Minéral 104: 582-586

Davis RJ, Hey MH (1969) The cell-contents of arthurite redetermined. Mineral Mag 37: 520-521.

Frost RL, Duong L, Martens W (2003) Molecular assembly in secondary minerals – Raman spectroscopy of the arthurite group species arthurite and whitmoreite. N Jb Mineral, Mh 2003: 223-240

Hughes JM, Bloodaxe ES, Kobel KD, Drexler JW (1996) The atomic arrangement of ojuelaite, $ZnFe^{3+}_2(AsO_4)_2(OH)_2.4H_2O$. Mineral Mag 60: 519-521

Jambor JL, Viñals J, Groat LA, Raudsepp M (2002) Cobaltarthurite, $CoFe^{3+}_2(AsO_4)_2(OH)_2.4H_2O$, a new member of the arthurite group. Can Mineral 40: 725-732

Kampf AR (2005) The crystal structure of cobaltarthurite from the Bou Azzer district, Morocco: the location of hydrogen atoms in the arthurite structure-type. Can Mineral 43: 1387-1391

Keller P, Hess H (1978) Die Kristallstruktur von Arthurit, $CuFe^{3+}_2[(H_2O)_4|(OH)_2|(PO_4)_2]$. N Jb Mineral, Abh 133: 291-302

Kolitsch U, Atencio D, Chukanov NV, Zubkova NV, Menezes Filho LAD, Coutinho JMV, Birch WD, Schlüter J, Pohl D, Kampf AR, Steele IM, Favreau G, Nasdala L, Möckel S, Giester G, Pushcharovsky YD (2010) Bendadaite, a new iron arsenate mineral of the arthurite group. Mineral Mag 74(3): 469-486

Libowitzky E (1999) Correlation of O-H stretching frequencies and O-H×××O hydrogen bond lengths in minerals. Monat Chem 130: 1047-1059

Matsubara S, Miyawaki R, Shigeoka M, Tajima H, Nishida K, Fujiwara Y (2009) Bendadaite and iron arsenate minerals from the Kiura mine, Oita Prefecture, Japan. 2009 Annual Meeting of Japan Association of Mineralogical Sciences, Abstracts Volume, Abs. R4-06, p. 100.

Meisser N (2010) Sur la présence de bendadaite à la Villatte-Haute (Monts d'Amabazac, Haute-Vienne). Le Règne Minéral 94: 40

Mielke Z, Ratajczak H (1972) The force constants and vibrational frequencies of orthoarsenates. Bulletin de l´Academie Polonaise des Sciences, Série des Sciences Chimiques 20: 265-270

Mills SJ, Kolitsch U, Birch WD, Sejkora J (2008) Kunatite, $CuFe_2(PO_4)_2(OH)_2 \cdot 4H_2O$, a new member of the whitmoreite group, from Lake Boga, Victoria, Australia. Austral J Mineral 14: 3-12

Mills SJ, Kampf AR, Sejkora J, Adams PM, Birch WD, Plášil J (2011) Iangreyite: a new secondary phosphate mineral closely related to perhamite. Mineral Mag 75: 327-336

Mills SJ, Sejkora J, Kampf AR, Grey IE, Bastow TJ, Ball NA, Adams PM, Raudsepp M, Cooper MA (2012) Krásnoite, the fluorophosphate analogue of perhamite, from the Huber open pit, Czech Republic and the Silver Coin mine, Nevada, USA. Mineral Mag 76: 625 - 634

Moore PB, Kampf AR, Irwing AJ (1974) Whitmoreite, $Fe^{2+}Fe^{3+}_2(OH)_2(H_2O)_4[PO_4]_2$, a new species: its description and atomic arrangement. Am Mineral 59: 900-905

Nakamoto K (2009) Infrared and Raman spectra of inorganic and coordination compounds Part A Theory and applications in inorganic chemistry. John Wiley and Sons Inc. Hoboken, New Jersey

Ondruš P (1993) ZDS - A computer program for analysis of X-ray powder diffraction patterns. Materials Science Forum, 133-136, 297-300, EPDIC-2. Enchede.

Palmer SJ, Frost RL (2011) The structure of the mineral arthurite $CuFe^{3+}(AsO_4,PO_4,SO_4)_2(OH)_2.4H_2O$. J Molec Struct 994: 283-288

Peacor DR, Dunn PJ, Simmons WB (1984) Earlshannonite, the Mn analogue of whitmoreite, from North Carolina. Can Mineral 22: 471-474

Pouchou JL, Pichoir F (1985) "PAP" (φρZ) procedure for improved quantitative microanalysis. In: Microbeam Analysis (J. T. Armstrong, ed.). San Francisco Press, San Francisco: 104-106

Raudsepp M, Pani E (2002) The crystal structure of cobaltarthurite, $Co^{2+}Fe^{3+}_2(AsO_4)_2(OH)_2 \cdot 4H_2O$: a Rietveld refinement. Can Mineral 40(2): 733-737

Rieck B, Kolitsch U, Voudouris P, Giester G, Tzeferis P (2018) Weitere Neufunde aus Lavrion, Griechenland. Mineralien-Welt 29(5): 32-77

Sejkora J, Ondruš P, Fikar M, Veselovský F, Mach Z, Gabašová A (2006a) New data on mineralogy of the Vysoký Kámen deposit near Krásno, Slavkovský les area, Czech Republic. J Czech Geol Soc 51: 43-55

Sejkora J, Ondruš P, Fikar M, Veselovský F, Mach Z, Gabašová A, Škoda R, Beran P (2006b) Supergene minerals at the Huber stock and Schnöd stock deposits, Krásno ore district, the Slavkovský les area, Czech Republic. J Czech Geol Soc 51: 57-101

Sejkora J, Škoda R, Ondruš P (2006c) New naturally occurring mineral phases from the Krásno-Horní Slavkov area, western Bohemia, Czech Republic. J Czech Geol Soc 51: 159–187

Sejkora J, Škoda R, Ondruš P, Beran P, Süsser C (2006d) Mineralogy of phosphate accumulations in the Huber stock, Krásno ore district, Slavkovský les area, Czech Republic. J Czech Geol Soc 5: 103-147

Sejkora J, Plášil J, Filip J (2011) Plimerite from Krásno near Horní Slavkov ore district, Czech Republic. J Geosci 56(2): 215-229

Sejkora J, Grey IE, Kampf AR, Price JR, Čejka J (2016) Tvrdýite, $Fe^{2+}Fe_2^{3+}Al_3(PO_4)_4(OH)_5(OH_2)_4 \cdot 2H_2O$, a new phosphate mineral from Krásno near Horní Slavkov, Czech Republic. Mineral Mag 80(6): 1077-1088

Staněk J (1988) Paulkerrite and earlshanonnite from pegmatite near Dolní Bory (western Moravia, Czechoslovakia). Čas Morav Muz, Vědy přír 73: 29-34

Staněk J (1997) Mineral associations of more significant pegmatite veins at Hatě near Dolní Bory, western Moravia. Acta Mus Morav, Sci natur 82: 3-19 (in Czech)

Vansant FK, Van Der Veken BJ, Desseyn HO (1973) Vibrational analysis of arsenic and its anions. I. Description of the Raman spectra. J Molec Struct 15: 425-437

Vrtiška L, Sejkora J, Malíková R (2018) Arthurite from Huber stock in Krásno near Horní Slavkov - the first occurrence in the Czech Republic. Bull Mineral Petrolog 26(1): 74-77 (in Czech)

Yvon K, Jeitschko W, Parthé E (1977) Lazy Pulverix, a computer program for calculation X-ray and neutron diffraction powder patterns. J Appl Cryst 10: 73-74